An experimental and theoretical study of the dynamics of grounding lines

SAMUEL S. PEGLER AND M. GRAE WORSTER

Institute of Theoretical Geophysics, Department of Applied Mathematics and Theoretical Physics, Wilberforce Road, Cambridge CB3 0WA, UK

(Received 30 July 2013)

We present an experimental and theoretical study of a thin, viscous fluid layer that flows radially under gravity from a point source into a denser inviscid fluid layer of uniform depth above a rigid horizontal surface. Near the source, the viscous layer lies in full contact with the surface, forming a vertical-shear-dominated viscous gravity current. At a certain distance from the source, the layer detaches from the surface to form a floating current whose dynamics are controlled by the viscous stresses due to longitudinal extension. We describe the dynamics of the grounded and floating components using distinct thin-layer theories. Separating the grounded and floating regions is the freely moving line of detachment, or grounding line, whose evolution we model by balancing the horizontal forces between the two regions. Using numerical and asymptotic analysis, we calculate the evolution of the system from a self-similar form at early times towards a steady state at late times. We use our solutions to illustrate how three-dimensional stresses within marine ice sheets, such as that of West Antarctica, can lead to stabilization of the grounding line. To assess the validity of the assumptions underlying our model, we compare its predictions with data from a series of laboratory experiments.

1. Introduction

Much of the West Antarctic Ice Sheet (WAIS) lies on bedrock up to two kilometres below sea level (Alley & Bindschadler 2001). Towards its interior, the ice sheet is thick enough to lie in full contact with the bedrock. However, as the ice sheet flows viscously under its own weight from the interior of the continent, it becomes vertically thinner and eventually detaches from the bedrock as a floating *ice shelf*. Separating the grounded part of the *ice sheet* and the ice shelf is the freely moving line of detachment called the *grounding line*. A *marine* ice sheet of this kind is naturally prone to instability because the gravity-driven spread of the flow towards the ocean acts to thin the ice sheet at the grounding line, causing the grounding line to retreat upstream. The retreat can be prevented only if there is a sufficient resupply of ice due to snowfall accumulation upstream of the grounding line, indicating that marine ice sheets are particularly sensitive to changes in climate. Retreating grounding lines have been observed in recent years (e.g. Wingham, Wallis & Shepherd 2009) and may be indications of a large-scale instability of the ice sheet, which alone has the potential to raise global sea level by several metres (Bamber *et al.* 2009).

Theoretical studies of the dynamics of marine ice sheets to date have focused on two-dimensional configurations in which the flow is idealized not to vary across its width (Weertman 1974; Wilchinsky & Chugunov 2000; Schoof 2007; Robison, Huppert & Worster 2010). In these studies, the sheet is modelled as a shear-dominated viscous

gravity current controlled by a balance between gradients in hydrostatic pressure and shear stresses due to friction at its base (Fowler & Larson 1978; Huppert 1982). By contrast, the absence of traction at the base of an ice shelf implies that shear stresses are not dominant there. Instead, the shelf undergoes a form of *extensional* viscous flow, characterized by experiencing only slight vertical shear and having leading-order dynamics that include viscous stresses due to longitudinal extension (Weertman 1957; DiPietro & Cox 1979; Robison *et al.* 2010; Pegler & Worster 2012; Pegler, Lister & Worster 2012). In cases where the sheet slides over the bedrock with only slight vertical shear, the transition between the sheet and shelf can be described by a so-called shallow-ice model, which simultaneously describes both the viscous stresses due to longitudinal extension and the frictional traction exerted at the base of the sheet (e.g. Schoof 2007). However, in cases where the friction at the base of the ice sheet is strong enough to induce significant vertical shear, all components of the stress tensor can be expected to become important near the grounding line (Nowicki & Wingham 2008), potentially leading to new dynamics not described by shallow ice models. Theoretical analysis of this case to date has focused on the asymptotic limit of small shear (Schoof 2011), on full-Stokes calculation of the steady flow (Nowicki & Wingham 2008) or on trying simplified descriptions of the dynamics in which certain viscous stresses are neglected (Robison *et al.* 2010).

The model of Robison *et al.* (2010) is developed under an assumption that viscous bending stresses, those due to horizontal gradients in vertical shear, do not contribute to the leading-order dynamics. This assumption leads to a model that describes the same kinds of physical balances as shallow-ice models, whilst allowing for a grounded sheet with dynamics dominated by vertical shear stresses. To test their theoretical model, Robison *et al.* (2010) conducted a laboratory study of an analogue two-dimensional marine ice sheet, the results of which showed some correlation with the model predictions. However, it was suggested that the results were significantly influenced by certain extraneous physical effects, one of which originated from the friction exerted by the side walls of their experimental tank (cf. Pegler 2012; Pegler *et al.* 2013).

In this paper, we extend previous studies by developing a theoretical model for a three-dimensional marine ice sheet and comparing its predictions with data from an analogue laboratory study. Our primary aim is to understand the essential dynamics associated with transitions between a shear-dominated sheet and an extension-dominated shelf, with our primary motivation to study a three-dimensional geometry stemming from the relative ease by which extraneous physics, such as side-wall effects, can be avoided in analogue laboratory experiments (cf. Robison *et al.* 2010). Specifically, we consider the axisymmetric flow of a marine ice sheet supplied at constant flux from a point source into an ocean of uniform depth. We build on the experimental study of Robison *et al.* (2010) by producing a confident benchmark against which our theoretical results can be compared, and evaluating the potential significance of physics not included in the model.

A further motivation for our analysis of radial flow is to elucidate new aspects of grounding-line dynamics introduced when a marine ice sheet spreads laterally in three dimensions. The axisymmetric geometry we consider provides a crude, yet illuminating model of the large-scale flow of ice from the interior of the Antarctic continent towards its periphery. One such aspect relates to the capacity for a radially flowing ice shelf to buttress the ice sheet at a curved grounding line, occurring as a consequence of the viscous hoop stresses associated with stretching the flow azimuthally (Pegler & Worster 2012). Such buttressing does not occur in two dimensions because the force exerted onto the ice sheet by the ice shelf is given simply by the hydrostatic pressure of the ocean transmitted along the shelf (Weertman 1974; Wilchinsky & Chugunov 2000; Schoof 2007; Robison *et al.* 2010).

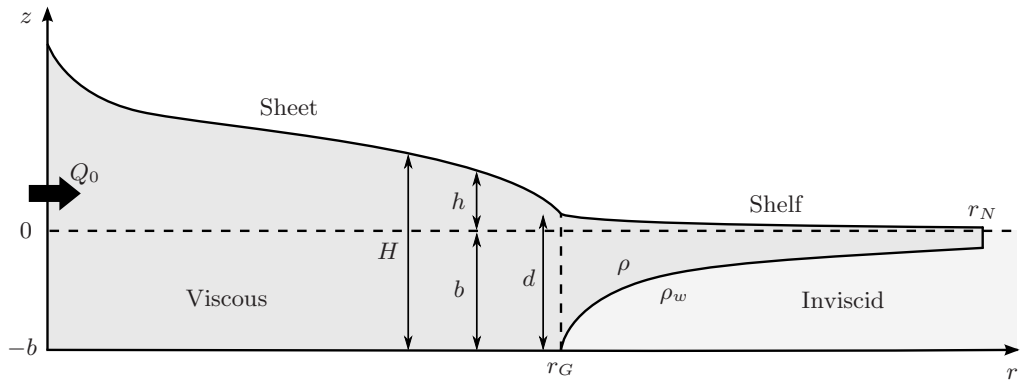

FIGURE 1. Cross-section of a radially flowing marine ice sheet.

A second, entirely separate, geometrical aspect introduced by radial flow relates to the possibility for the grounding line to converge towards a steady position on horizontal bedrock or on topography that slopes upwards in the direction of the flow. It has been well-documented that the grounding line of an idealized two-dimensional marine ice sheet cannot converge towards a steady position on such topography (e.g. Weertman 1974). Indeed, most of the bedrock below the interior of the WAIS slopes upwards in the direction of the flow, a feature that has formed the basis for speculation that the WAIS is inherently unstable (Bamber *et al.* 2009). Here, we address whether this hypothesis of instability holds in more general three-dimensional settings.

We begin in §2 by developing our model for an idealized marine ice sheet that flows radially from a point source. In §3, we explore solutions to the model system using asymptotic and numerical approaches. In §4, we present our laboratory study and compare the experimental data with our theoretical predictions. Finally, in §5 we discuss the implications of this comparison and conclude in §6 by summarizing our results.

2. Theoretical model

Consider a layer of viscous Newtonian fluid of density ρ and viscosity μ flowing radially into an effectively infinite layer of inviscid fluid of larger density ρ_w, which rests on a rigid surface $z = -b(r)$, shown schematically in figure 1. The viscous fluid layer can be considered in two regions: the grounded *sheet*, which lies in contact with the lower surface; and the floating *shelf*, which floats on the inviscid fluid. These are separated by the circular line of detachment $r_G(t)$ called the *grounding line*. Let $H(r,t)$ and $h(r,t)$ denote the thickness of the layer and the height of its upper surface above that of the inviscid fluid $z = 0$, respectively. These can be related to one another by

$$h = \begin{cases} H - b & (r < r_G), \\ (\rho_w - \rho)H/\rho_w & (r > r_G), \end{cases} \qquad (2.1a,b)$$

(cf. Weertman 1974; Robison *et al.* 2010; Pegler *et al.* 2013). Equation (2.1a) follows from the fact that the vertical position of the base of the sheet is set simply by the geometry of the underlying surface. Equation (2.1b) follows from an assumption that the vertical position of the shelf is set by Archimedes principle, applicable if viscous bending stresses are negligible and the vertical component of stress $\sigma_{zz} = \rho g(z - h)$ is purely hydrostatic (e.g. Pegler & Worster 2012).

2.1. *Grounded sheet*

Far upstream of the grounding line, the sheet forms a shear-dominated viscous gravity current (cf. Robison *et al.* 2010). The leading-order dynamics of such a current involve a balance between the divergence of vertical shear stresses and the gradients in hydrostatic pressure caused by the slope of its upper surface, described by

$$\mu\frac{\partial^2 u}{\partial z^2} = \rho g\frac{\partial h}{\partial r}, \tag{2.2}$$

where u is the horizontal velocity (Huppert 1982). Integrating (2.2) subject to the condition of no slip at the base of the current ($u = 0$ at $z = -b$) and the leading-order condition of no stress at the free surface ($\mu\partial u/\partial z = 0$ at $z = h$), we obtain the parabolic-shear profile

$$u = -\frac{g}{2\nu}(z+b)\big[2H - (z+b)\big]\frac{\partial h}{\partial r}, \tag{2.3}$$

where $\nu \equiv \mu/\rho$ is the kinematic viscosity. Given (2.3), the evolution of the thickness of the sheet H is described by the depth-integrated continuity equation

$$\frac{\partial H}{\partial t} + \frac{1}{r}\frac{\partial}{\partial r}(rq) = 0, \quad \text{where} \quad q \equiv \int_{-b}^{h} u\,\mathrm{d}z = -\frac{g}{3\nu}H^3\frac{\partial h}{\partial r} \tag{2.4a,b}$$

is the velocity (2.3) integrated across the depth of the flow. Substitution of (2.4b) into (2.4a) determines the governing nonlinear diffusion equation

$$\frac{\partial H}{\partial t} = \frac{g}{3\nu}\frac{1}{r}\frac{\partial}{\partial r}\left(rH^3\frac{\partial h}{\partial r}\right). \tag{2.5}$$

Assuming that the sheet is supplied at a constant rate at $r = 0$, we impose

$$\lim_{r\to 0}(2\pi rq) = \lim_{r\to 0}\left(-\frac{2\pi g}{3\nu}rH^3\frac{\partial h}{\partial r}\right) = Q_0, \tag{2.6}$$

where Q_0 is the volumetric flux, and the first equation follows on using (2.4b) to substitute for q.

We assume that the grounding line r_G lies at the first radius at which the sheet has thinned sufficiently for hydrostatic flotation to apply there (Weertman 1974; Schoof 2007; Robison *et al.* 2010). This assumption is equivalent to applying continuity of the height h at r_G in (2.1), furnishing the *flotation condition*,

$$H(r_G, t) = \frac{\rho_w}{\rho}b(r_G) \equiv d(r_G), \tag{2.7}$$

where d is the *flotation thickness*. For ice floating on water, $\rho_w/\rho \approx 1.1$.

The grounding line $r_G(t)$ is a freely moving boundary, so a further condition, in addition to (2.6) and (2.7), is needed in order to solve the second-order equation (2.5) for the evolution of H and r_G. We determine this final condition later in §2.3 by applying a force balance between the sheet and the shelf.

2.2. *Floating shelf*

In the absence of any tangential stress exerted at its upper and lower surfaces, the shelf forms an axisymmetric extensional viscous gravity current (Pegler & Worster 2012; Pegler *et al.* 2012). The radial velocity $u(r, t)$ of such a current is governed to leading order by

$$\frac{\partial}{\partial r}\left[H\left(\boldsymbol{\nabla}\cdot\boldsymbol{u} + e_{rr}\right)\right] + \frac{H}{r}(e_{rr} - e_{\theta\theta}) = \frac{g'}{2\nu}H\frac{\partial H}{\partial r}, \tag{2.8}$$

where $e_{rr} = \partial u/\partial r$ and $e_{\theta\theta} = u/r$ are the rates of radial and azimuthal extension, respectively, $g' \equiv (\rho_w - \rho)g/\rho_w$ is the reduced gravity and $\boldsymbol{\nabla}$ is the horizontal gradient operator. Significant mathematical contrast can be drawn between (2.8) and the equation that determines u in the case of a shear-dominated viscous gravity current (2.3). In the former, u depends on the thickness H throughout the current. In the latter, u depends only on the local surface height and its gradient.

Having obtained u from an integration of (2.8) subject to suitable boundary conditions on u, the evolution of the thickness H is described by the depth-integrated form of the continuity equation,

$$\frac{\partial H}{\partial t} + \frac{1}{r}\frac{\partial}{\partial r}\left(rHu\right) = 0. \tag{2.9}$$

Applying continuity conditions on the flux q and the thickness H across the grounding line, we impose

$$q_+ = q, \qquad H_+ = H \qquad (r = r_G), \tag{2.10a,b}$$

(cf. Robison *et al.* 2010; Pegler *et al.* 2013). To distinguish between quantities evaluated in the shelf and the sheet at the grounding line, here we have used a + subscript to denote a shelf quantity and absence of the subscript to denote a sheet quantity, a convention that we use from now on. Condition (2.10b) provides an initial condition on the characteristics of the hyperbolic equation (2.9). Note that, in their analysis of a laterally confined marine ice sheet, Pegler *et al.* (2013) apply a condition of identical form to (2.10b), but because of the nature of the shear-dominated flow of the shelf in that problem, its role there is not to provide an initial condition but to balance the leading-order hydrostatic stresses across the grounding line. Here, (2.10b) does not imply a leading-order force balance because, as is characteristic of transitions towards regimes that include significant extensional stresses, the viscous contributions to the longitudinal stress form the most significant contribution to the leading-order balance of forces (see §2.3 below and cf. Schoof 2007; Robison *et al.* 2010; Pegler 2012).

Combining (2.10a, b), we determine the entry-velocity condition for the shelf

$$u_+ = \frac{q}{H} \qquad (r = r_G), \tag{2.11}$$

which provides one boundary condition for solution of (2.8) for u. A second is given by the frontal stress condition

$$2\frac{\partial u}{\partial r} + \frac{u}{r} = \frac{g'}{4\nu}H \qquad (r = r_N), \tag{2.12}$$

where r_N denotes the frontal position of the shelf (Pegler & Worster 2012). Finally, conservation of mass applied at the front implies that its position evolves according to

$$\dot{r}_N = u(r_N, t). \tag{2.13}$$

2.3. *Grounding line*

As we have noted above, the system of equations (2.5)–(2.7) is not closed. Missing is a condition that determines the rate of change of the grounding-line position $\dot{r}_G$. If we differentiate the flotation condition (2.7) with respect to time, we obtain

$$\dot{r}_G\frac{\partial H}{\partial r} + \frac{\partial H}{\partial t} = \dot{r}_G\frac{\mathrm{d}d}{\mathrm{d}r} \qquad (r = r_G), \tag{2.14}$$

which shows that the advancement or recession of the grounding line is associated with the thickening or thinning of the sheet ($\partial H/\partial t$) there. Using (2.4a) to substitute for

$\partial H/\partial t$ in favour of the divergence of flux $\boldsymbol{\nabla}\cdot\boldsymbol{q}$, where $\boldsymbol{q}\equiv q\hat{\boldsymbol{r}}$, we determine further that

$$\dot{r}_G\left(\frac{\mathrm{d}d}{\mathrm{d}r}-\frac{\partial H}{\partial r}\right)=\frac{\partial H}{\partial t}=-\boldsymbol{\nabla}\cdot\boldsymbol{q}\qquad(r=r_G). \tag{2.15}$$

Equation (2.15) shows that a determination of the grounding-line velocity $\dot{r}_G$ is equivalent to a boundary condition on the divergence of flux $\boldsymbol{\nabla}\cdot\boldsymbol{q}$ at the grounding line.

In physical terms, it is clear that a calculation of $\boldsymbol{\nabla}\cdot\boldsymbol{q}$ must depend on a balance of forces between the sheet and the shelf. Were one to stretch the shelf by pulling its front forwards, the flow at the grounding line would also stretch, increasing $\boldsymbol{\nabla}\cdot\boldsymbol{q}$ and causing the sheet to thin. Conversely, were one to push the front of the shelf towards the grounding line, $\boldsymbol{\nabla}\cdot\boldsymbol{q}$ would decrease, causing thickening of the sheet there and advancement of the grounding line.

The two models presented in §§2.1–2.2 above can be expected to describe the leading-order evolution of the sheet and shelf only sufficiently far behind or in front of the grounding line, respectively. The shear-dominated model of the sheet, in particular, neglects the extensional stresses that necessarily become significant to connect the flow to the extensional shelf near the grounding line. There must therefore be a *transition region* near the grounding line in which that model no longer applies to leading order (cf. Weertman 1974; Schoof 2007). By forming a scaling between the stresses due to vertical shear ($\mu\,\partial u/\partial z$) implied by (2.3) and those due to longitudinal extension ($\mu\,\partial u/\partial r$) in (2.8) and (2.12), we find that the extent of this transition region can be characterized by the length scale

$$L\equiv\left(\frac{g}{g'}\right)^{1/2}d(r_G), \tag{2.16}$$

increasing linearly with the thickness of the layer at the grounding line $d(r_G)$. The dimensionless prefactor $(g/g')^{1/2}\approx 3.5$ is of order unity for ice intruding water, in which case L is effectively the thickness of the layer at the grounding line. The extent of the transition region (2.16) can be expected to be applicable to any transition from a shear-dominated gravity current to one of extension (it is not specific to our axisymmetric geometry).

Strictly then, the shear-dominated model of §2.1 applies only for $|r_G-r|\gg L$, with the transition region $|r_G-r|\ll L$ providing a boundary layer in which extensional stresses become significant (cf. Schoof 2007). A formal calculation of $\boldsymbol{\nabla}\cdot\boldsymbol{q}$, needed in (2.15), should therefore be achieved by considering a model that can account for both vertical-shear and extensional stresses simultaneously (e.g. Nowicki & Wingham 2008). Here, we instead adopt a simpler approach by neglecting the extensional stresses in the sheet all the way up to the grounding line or, in other words, by patching the horizontal forces between the upstream, shear-dominated regime of the sheet and the downstream extensional shelf (cf. Robison *et al.* 2010). Thus, we apply

$$F_+=F,\quad\text{where}\quad F\equiv\int_{h-H}^{h}\sigma_{rr}\,\mathrm{d}z\qquad(r=r_G) \tag{2.17a,b}$$

is the horizontal force per unit width exerted by a vertical cross-section of the flow. While not strictly leading-order, this modelling approach can be expected to be of similar accuracy to a model that also accounts for the extensional stresses in the transition region towards the front of the sheet (Pegler 2012), whilst describing the important physics in simpler and more illuminating terms.

For thin viscous layers in which the leading-order vertical stress is hydrostatic, $\sigma_{zz}=\rho g(z-h)$, applicable to both our model of the sheet and the shelf (Huppert 1982; Pegler

& Worster 2012), the horizontal force exerted by the layer (2.17*b*) can be evaluated as

$$F = -\tfrac{1}{2}\rho g H^2 + 2\mu \int_{h-H}^{h} \boldsymbol{\nabla}\cdot\boldsymbol{u} + e_{rr}\,\mathrm{d}z, \tag{2.18}$$

(Pegler & Worster 2012). In the sheet, we use (2.3) to substitute for u in (2.18) and determine that

$$\begin{aligned} F &= -\tfrac{1}{2}\rho g H^2 + 2\mu \int_{-b}^{h} \frac{1}{r}\frac{\partial (ru)}{\partial r} + \frac{\partial u}{\partial r}\,\mathrm{d}z \qquad (r = r_G), \\ &= -\tfrac{1}{2}\rho g H^2 + 2\mu \left\{ \left[\frac{g}{\nu} H^2 \left(\frac{\partial h}{\partial r} \right)^2 - \frac{q}{r} \right] + 2\boldsymbol{\nabla}\cdot\boldsymbol{q} \right\} \qquad (r = r_G), \end{aligned} \tag{2.19}$$

which shows that the force exerted by the sheet has three distinct contributions: the depth-integrated hydrostatic pressure; the contribution to the divergence of flux due to the advection of the flow; and lastly, the viscous extensional stress associated with the divergence of the flux at the grounding line. The first term, representing the depth-integrated hydrostatic pressure, is the largest contribution to F. However, as shown below, this contribution simply balances a corresponding contribution from the shelf, and it is the other (viscous) contributions to F that ultimately determine $\boldsymbol{\nabla}\cdot\boldsymbol{q}$.

In the shelf, (2.18) can be evaluated as (Pegler & Worster 2012)

$$\begin{aligned} F_+ &= -\tfrac{1}{2}\rho g H^2 + 2\mu H \left[\boldsymbol{\nabla}\cdot\boldsymbol{u} + e_{rr}\right]_+ \qquad (r = r_G), \\ &= -\tfrac{1}{2}\rho g H^2 + \left[\tfrac{1}{2}\rho g' H^2 + 2\mu \int_{r_G}^{r_N} H \frac{\partial}{\partial r}\left(\frac{u}{r} \right) \mathrm{d}r \right] \qquad (r = r_G), \end{aligned} \tag{2.20}$$

which is the sum of three contributions: the depth-integrated hydrostatic pressure; the discontinuity in depth-integrated hydrostatic pressures between the layer and the ocean; and the *buttressing* associated with balancing the hoop stresses throughout the shelf. The presence of the buttressing integral in (2.20) implies that F_+ depends on the full distributions of the thickness H and velocity u throughout the shelf. This can be contrasted with two-dimensional models (e.g. Schoof 2007; Robison *et al.* 2010), where only the thickness of the layer at the grounding line determines the force exerted onto the front of the sheet and an explicit consideration of the downstream dynamics of the shelf are irrelevant (as would be true here also if the buttressing integral in (2.20) were absent).

Substitution of (2.19) and (2.20) into (2.17*a*) gives

$$2\boldsymbol{\nabla}\cdot\boldsymbol{q} - \frac{q}{r} + \frac{g}{\nu} H^2 \left(\frac{\partial h}{\partial r} \right)^2 = \frac{g'}{4\nu} H^2 + \int_{r_G}^{r_N} H \frac{\partial}{\partial r}\left(\frac{u}{r} \right) \mathrm{d}r \qquad (r = r_G), \tag{2.21}$$

yielding the desired boundary condition on $\boldsymbol{\nabla}\cdot\boldsymbol{q}$ needed to close the integration of the sheet equations. Using (2.21) to evaluate $\boldsymbol{\nabla}\cdot\boldsymbol{q}$ in (2.15), we obtain finally an explicit equation for the evolution of the grounding line,

$$\dot{r}_G = \dot{r}_{\mathrm{dyn}} \equiv \frac{\dfrac{g}{2\nu} H^2 \left(\dfrac{\partial h}{\partial r} \right)^2 - \dfrac{q}{2r} - \dfrac{g'}{8\nu} H^2 - \dfrac{1}{2} \displaystyle\int_{r_G}^{r_N} H \frac{\partial}{\partial r}\left(\frac{u}{r} \right) \mathrm{d}r}{\dfrac{\mathrm{d}d}{\mathrm{d}r} - \dfrac{\partial H}{\partial r}} \qquad (r = r_G). \tag{2.22}$$

Equation (2.22) shows how the grounding line responds to the forces that balance the divergence of the flux in (2.21). The denominator converts the change in H implied by the numerator into a change in grounding-line position, such as to maintain the flotation condition (2.7). The sum of the first two terms in the numerator, which together repre-

sent the advective contribution to the divergence of flux, is typically positive, reflecting the fact that a greater flow of fluid towards the grounding line promotes grounding-line advancement. The third term, representing the discontinuity in hydrostatic pressure between the front of the sheet at the grounding line and the ocean, is always negative, since a fluid layer satisfying Archimedean flotation naturally spreads outwards under horizontal gradients in buoyancy (e.g. Pegler *et al.* 2012), promoting grounding-line recession. The last term in the numerator represents the buttressing exerted by the shelf. This can be either positive or negative depending on the curvature of the grounding line and the acceleration of the flow in front of it (Pegler & Worster 2012).

If the surface slope of the sheet $\partial h/\partial x$ is sufficiently steep, it is possible for (2.22) to predict that $H\dot{r}_G > q$, such that the grounding line advances too quickly for fluid to be supplied towards it (cf. Robison *et al.* 2010). In such cases, we assume instead that the grounding line advances at the largest velocity permitted by the constraint $H\dot{r}_G \leq q$. Thus, we impose

$$\dot{r}_G = \min\{\dot{r}_{\rm dyn}, \dot{r}_{\rm kin}\}, \quad \text{where} \quad \dot{r}_{\rm kin} \equiv \frac{q}{H} = -\frac{g}{3\nu}H^2\frac{\partial h}{\partial r} \qquad (2.23a,b)$$

is the *kinematic* grounding-line velocity.

2.4. *Shelf formation*

The dynamic grounding-line velocity (2.22) was derived under the assumption that the shelf had already formed. Before the shelf forms, however, it is necessary to determine whether the front of the sheet evolves kinematically according to (2.23*b*), or whether the shelf forms and the grounding line evolves dynamically according to (2.22). This question can be answered by checking whether the introduction of a short, nascent shelf would lead to a dynamic velocity (2.22) that is consistent with the front of the shelf propagating faster than the grounding line ($\dot{r}_{\rm dyn} < \dot{r}_{\rm kin}$). In order to perform this check efficiently, we proceed to develop a simplified form for (2.22) in the asymptotic limit of a short shelf ($r_N \to r_G^+$). In this limit, the effectively infinitesimal extent of the shelf implies that it only transmits the hydrostatic pressure of the ocean to the grounding line (the buttressing integral in (2.20) is vanishingly small). In other words, the hypothetical dynamic grounding-line velocity that would apply if the shelf were to form is equivalent to (2.22), but without the buttressing integral, so

$$\dot{r}_{\rm dyn} = \left(\frac{g}{2\nu}H^2\left(\frac{\partial h}{\partial r}\right)^2 - \frac{q}{2r} - \frac{g'}{8\nu}H^2\right) \Big/ \left(\frac{{\rm d}d}{{\rm d}r} - \frac{\partial H}{\partial r}\right) \qquad (r_N \to r_G^+). \qquad (2.24)$$

By substituting (2.24) and (2.23*b*) into the inequality $\dot{r}_{\rm dyn} < \dot{r}_{\rm kin}$, we determine the criterion for when the shelf is able to form as

$$\frac{g}{2\nu}H^2\left(\frac{\partial h}{\partial r}\right)^2 - \frac{q}{2r} - \frac{g'}{8\nu}H^2 < \frac{q}{H}\left(\frac{{\rm d}d}{{\rm d}r} - \frac{\partial H}{\partial r}\right) \qquad (r = r_G). \qquad (2.25)$$

Once (2.25) is satisfied, we initialize a nascent shelf in a small interval $[r_G, r_N]$ in front of the grounding line. In order to achieve this effectively, we proceed to develop an asymptotic approximation for the nascent shelf by, yet again, considering the limit $r_N \to r_G^+$. Anticipating that the leading-order thickness and velocity profiles of the nascent shelf are both linear, we write them as Taylor expansions, namely,

$$H \sim d(r_G) + (r - r_G)\left.\frac{\partial H}{\partial r}\right|_+, \qquad u \sim u_+ + (r - r_G)\left.\frac{\partial u}{\partial r}\right|_+, \qquad (2.26a,b)$$

respectively, where the neglected terms are $O([r_N - r_G]^2)$. On substitution of (2.26*a*, *b*)

into (2.11) and (2.12), the leading-order velocity and rate of extension of the nascent shelf are found to be given by

$$u_+ \sim \frac{q}{d}, \qquad \left.\frac{\partial u}{\partial r}\right|_+ \sim \frac{g'}{8\nu}d - \frac{u_+}{2r_G}, \tag{2.27}$$

respectively. Expanding the continuity equation (2.9) using the product rule and substituting for H and u using (2.26)–(2.27), we determine that the leading-order thickness gradient of the nascent shelf $a(t) \equiv \partial H/\partial r|_+$, appearing in (2.26$a$), evolves according to

$$\dot{r}_G \frac{\mathrm{d}d}{\mathrm{d}r} + [u_+ - \dot{r}_G]a + [r - r_G]\dot{a} \sim -\frac{g'}{8\nu}d^2 - \frac{q}{2r_G}. \tag{2.28}$$

Noting that the last term on the left-hand side of (2.28) is of higher order, we neglect this term and determine finally that the leading-order thickness gradient of the shelf is

$$\left.\frac{\partial H}{\partial r}\right|_+ \equiv a \sim \left(-\frac{g'}{8\nu}d^2 - \frac{q}{2r_G} - \frac{\mathrm{d}d}{\mathrm{d}r}\dot{r}_G\right) \Big/ (u_+ - \dot{r}_G). \tag{2.29}$$

3. Theoretical analysis

The system of equations given by (2.5)–(2.13) and (2.22)–(2.23) describes the evolution of the layer for topography of the general form $b(r)$. We proceed to analyse the illustrative example of a horizontal bedrock, specified by setting the flotation thickness (2.7) to a uniform value, so

$$d \equiv d_0. \tag{3.1}$$

In this case, the system depends on the four independent parameters Q_0, g/ν, g'/g, and d_0. By forming scalings between terms in the governing equations (2.5)–(2.13), we determine the intrinsic scales of thickness, time and horizontal length,

$$\mathcal{H} \equiv \left(\frac{\nu Q_0}{2\pi g}\right)^{1/4}, \qquad \mathcal{T} \equiv \frac{\nu}{g'\mathcal{H}}, \qquad \mathcal{L} \equiv \left(\frac{g}{g'}\right)^{1/2}\mathcal{H}, \tag{3.2a,b,c}$$

respectively. Here, (3.2a) characterizes the thickness of an axisymmetric viscous gravity current supplied over a horizontal surface at constant volumetric flux (Huppert 1982). If the thickness of the sheet is characterized by $\mathcal{H}$, then (3.2b,c) characterize the time and horizontal extent on which buoyancy forces have significant influence on the dynamics of the sheet. We use (3.2a,b,c) to make the system dimensionless according to

$$r \equiv \mathcal{L}\hat{r}, \quad t \equiv \mathcal{T}\hat{t}, \quad H \equiv \mathcal{H}\hat{H}, \quad u \equiv (\mathcal{L}/\mathcal{T})\hat{u}. \tag{3.3}$$

With hats dropped, the equation of the sheet (2.5) becomes

$$\frac{\partial H}{\partial t} = \frac{1}{3r}\frac{\partial}{\partial r}\left(rH^3\frac{\partial H}{\partial r}\right), \tag{3.4}$$

and boundary conditions (2.6) and (2.7) become

$$\lim_{r\to 0}\left(-\frac{1}{3}rH^3\frac{\partial H}{\partial r}\right) = 1, \quad H(r_G, t) = D, \tag{3.5a,b}$$

respectively. The equations of the shelf (2.8)–(2.9) become

$$\frac{\partial}{\partial r}\left[H\left(2\frac{\partial u}{\partial r}+\frac{u}{r}\right)\right]+H\frac{\partial}{\partial r}\left(\frac{u}{r}\right)=\frac{1}{2}H\frac{\partial H}{\partial r}, \tag{3.6}$$

$$\frac{\partial H}{\partial t}+\frac{1}{r}\frac{\partial}{\partial r}\left(rHu\right)=0, \tag{3.7}$$

and boundary conditions (2.10b) and (2.13) become

$$H_+=D \qquad u_+=\frac{q}{H} \qquad (r=r_G), \tag{3.8a,b}$$

$$2\frac{\partial u}{\partial r}+\frac{u}{r}=\frac{1}{4}H, \qquad \dot{r}_N=u \qquad (r=r_N), \tag{3.9a,b}$$

respectively. The grounding-line evolution equations (2.22)–(2.23) become

$$\dot{r}_{\rm dyn}=\left(\frac{1}{2}H^2\left(\frac{\partial H}{\partial r}\right)^2-\frac{q}{2r}-\frac{1}{8}H^2-\frac{1}{2}\int_{r_G}^{r_N}H\frac{\partial}{\partial r}\left(\frac{u}{r}\right)\mathrm{d}r\right)\Big/\left(-\frac{\partial H}{\partial r}\right), \tag{3.10}$$

$$\dot{r}_{\rm kin}=-\frac{1}{3}H^2\frac{\partial H}{\partial r}. \tag{3.11}$$

Finally, the criterion for when the shelf is able to form (2.25) takes the simplified dimensionless form

$$\left(\frac{\partial H}{\partial r}\right)^2+\frac{H}{r}\frac{\partial H}{\partial r}-\frac{3}{4}<0 \qquad (r=r_G). \tag{3.12}$$

The system above depends on the single dimensionless parameter

$$D\equiv d_0/\mathcal{H}, \tag{3.13}$$

appearing in (3.5b) and (3.8a), which is a *dimensionless flotation thickness*.

Two illustrative numerical solutions to the system above are shown in figures 2(a, b) in the cases $D=1$ and $D=2$, respectively. With $D=1$, the system is initially composed only of a sheet, with a frontal position that initially evolves kinematically according to (3.11). At $t\approx 2.04$, (3.12) is satisfied and the grounding line proceeds to evolve dynamically according to (3.10), with a shelf extending in front of it. The switch in grounding-line control from kinematic to dynamic when $\dot{r}_{\rm kin}$ first exceeds $\dot{r}_{\rm dyn}$ is illustrated in figure 2(c). At later times ($t\gtrsim 50$), the system converges towards a steady state, indicated by the dotted curve. With the larger dimensionless flotation thickness $D=2$, the sheet and shelf both form simultaneously at the initiation of the source, with $\dot{r}_{\rm dyn}$ smaller than $\dot{r}_{\rm kin}$ at all times, as indicated in figure 2(c). The shelf proceeds to occupy a significantly larger proportion of the domain than the sheet, as compared to the case $D=1$. There is also a dramatic contrast in grounding-line position and rate of convergence towards steady flow between $D=1$ and $D=2$, reflecting the extreme sensitivity of the flow to this parameter. The grounding-line position r_G and frontal position r_N are seen in figure 3 to evolve as $t^{1/2}$ at early times, albeit with some markedly different prefactors. At late times, the grounding line converges towards a steady position, but the frontal position r_N instead accelerates to become linear with time.

3.1. *Early evolution*

In analysing the early evolution of the system, we begin by presupposing that the system is initially composed of a sheet only, as was illustrated to occur in the case $D=1$ above. The self-consistency of this early-time regime will be determined *a posteriori*.

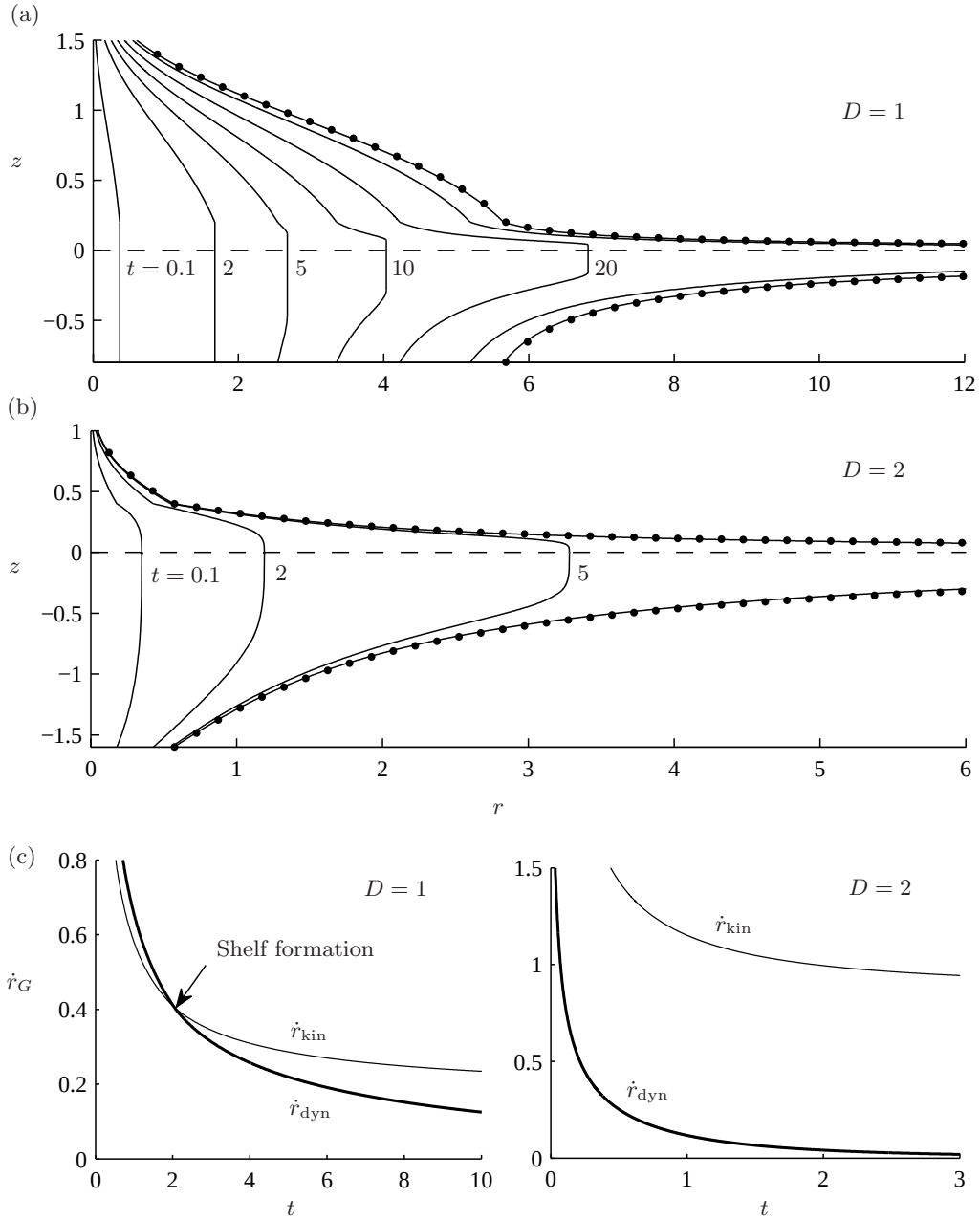

FIGURE 2. Evolution of the surface profiles with (a) $D = 1$ and (b) $D = 2$ shown at dimensionless times of $t = 0.1, 2, 5$ and 10, and the additional times of $t = 20, 50$, and 200 in (a). In the case $D = 1$, the grounding line is controlled kinematically according to (3.11) until $t \approx 2.04$ when the shelf forms, and the grounding line is subsequently controlled dynamically according to (3.10). By contrast, the shelf forms immediately in the case $D = 2$, with an early-time flow comprised of both a sheet and a shelf. The asymptotic steady states determined in §3.2 are shown as dotted curves. (c) The evolutions of the dynamic and kinematic grounding-line velocities (3.10)–(3.11) for $D = 1$ and 2.

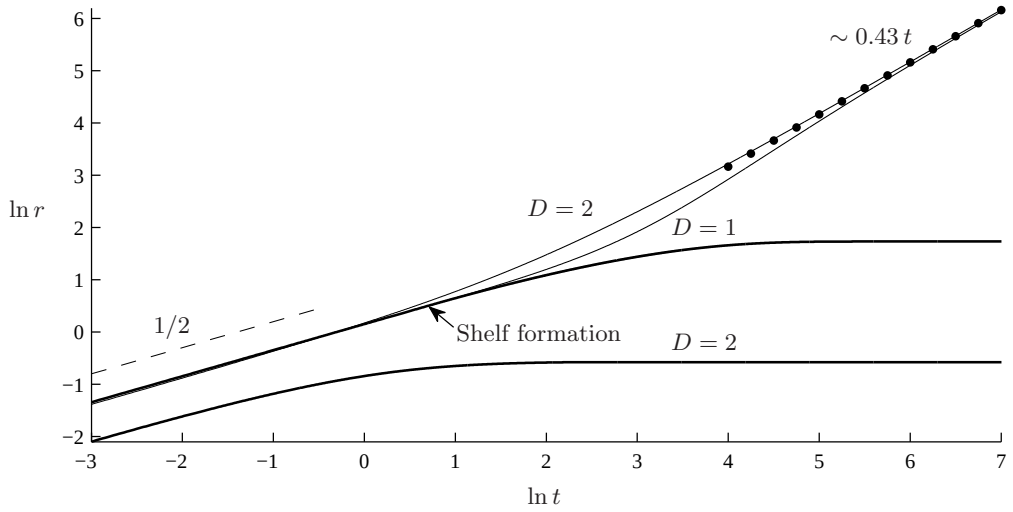

FIGURE 3. Evolution of the grounding line $r_G(t)$ (thick) and shelf front $r_N(t)$ (thin) in the two cases $D = 1$ and 2. Each evolves as $t^{1/2}$ at early times, corresponding to the self-similar evolution described in §3.1. In the case $D = 1$, the shelf forms at time $t \approx 2.04$, indicated by an arrow. The shelf forms immediately at $t = 0$ in the case $D = 2$. In both cases, the frontal position r_N converges towards the asymptote (3.23*b*) (dotted).

3.1.1. *Delayed shelf formation*

If the grounding line evolves kinematically according to (3.11), with the shelf yet to form, then the system is described by (3.4), (3.5) and (3.11) only. In order to form a horizontal length scale from these equations, it is necessary to incorporate an explicit dependence on t, indicating that an initial regime of this kind can be described by a similarity solution. Motivated by a scaling analysis of the equations, we define similarity variables according to

$$\eta \equiv t^{-1/2} r, \quad H \equiv f(\eta), \tag{3.14}$$

implying that the frontal position evolves according to $r_G = \eta_G t^{1/2}$, where η_G is a constant (cf. Huppert 1982). In terms of (3.14), the equation of the sheet (3.4) becomes

$$-\tfrac{1}{2}\eta^2 f' = \tfrac{1}{3}(\eta f^3 f')', \tag{3.15}$$

where we have used a prime here to denote $\mathrm{d}/\mathrm{d}\eta$. Conditions (3.5*a*, *b*) and (3.11) become

$$\lim_{\eta\to 0}\left(-\tfrac{1}{3}\eta f^3 f'\right) = 1, \quad f(\eta_G) = D, \quad f'(\eta_G) = -\tfrac{3}{2}\eta_G D^{-2}, \tag{3.16a,b,c}$$

respectively. Equations (3.15)–(3.16) generalize those describing an axisymmetric viscous gravity current over a horizontal surface (Huppert 1982) to allow for a non-vanishing frontal thickness (3.16*b*). We solve (3.15)–(3.16) numerically using a fourth-order Runge-Kutta scheme in which η_G is treated as a shooting parameter. Our solution with $D = 1$, shown in figure 4(*a*), exhibits a shape characteristic of axisymmetric viscous gravity currents upstream of the front, including the logarithmic singularity

$$f \sim [12\ln(1/\eta)]^{1/4} \qquad (\eta \to 0), \tag{3.17}$$

obtained from an integration of the near-field profile implied by (3.16*a*) (Huppert 1982). In contrast, however, the front of the layer is vertical to leading order and the slope of the surface towards it is finite.

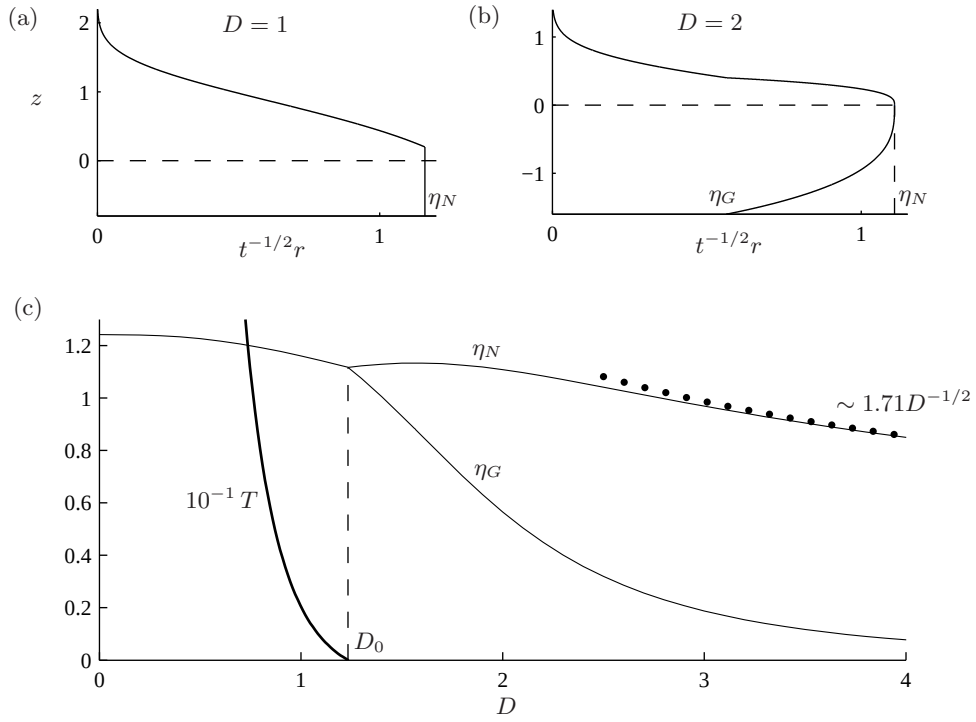

FIGURE 4. Early-time similarity solutions for (a) $D = 1$, and (b) $D = 2$. Panel (c) shows the time of shelf formation T and the similarity coordinates of the position of the grounding line η_G and shelf front η_N each plotted against the dimensionless flotation thickness D. The critical value $D_0 \approx 1.23$ separates the cases of delayed and immediate shelf formation, as outlined in §3.1. The large-D asymptote (3.22) for η_N is plotted as a dotted curve in (c).

Substituting (3.14) into the critical case of the shelf-formation criterion (3.12), with f and f' evaluated using (3.16b, c), we determine the time of shelf formation as

$$T = 3\eta_G^2 D^{-4} - 2D^{-1}, \tag{3.18}$$

which we have plotted as a thick curve in figure 4(c). Once $t > T$, the criterion (3.12) is satisfied and the dynamic grounding-line velocity (3.10) can be applied without causing the grounding line to overtake the front of the shelf (see §2.4). The switch to dynamic grounding-line control introduces the length scale (3.2c) into the system, reflecting the presence of the buoyancy gradient in (3.10), and precluding any subsequent self-similarity. Tracking (3.18) as D is increased, we find that it vanishes ($T = 0$) at the critical value $D = D_0 \approx 1.23$ – see figure 4(c). The similarity solution calculated above therefore predicts that the shelf-formation criterion (3.12) is satisfied immediately at $t = 0$ if $D > D_0$, such that it is inconsistent with (2.23a). To address the early-time flow for such D, we instead survey the possibility of an early-time regime in which the dynamic condition (3.10) applies.

3.1.2. *Immediate shelf formation*

If the shelf occupies the region near the source ($r_N \ll 1$) then the dimensionless velocity imposed at the grounding line ($u \sim r_G^{-1}$) is very much larger than the dimensionless velocity ($u \sim 1$) on which buoyancy drives the flow (Pegler & Worster 2012). In this limit, the buoyancy forces on the right-hand sides of (3.6) and (3.9a) are therefore negligible and the leading-order force balance throughout the shelf is purely viscous. In the absence

of the buoyancy forces in the shelf, a horizontal length scale cannot be formed from the full system of equations describing the sheet and shelf (3.4)–(3.11), indicating that the full sheet–shelf system can be described by a similarity solution for $t \ll 1$.

In terms of (3.14), the equations describing the sheet (3.4)–(3.5) become (3.15) and (3.16a, b), as above. The shelf equations (3.6)–(3.7) become

$$(fs')' + f\left(\frac{s}{\eta}\right)' + \frac{f's}{2\eta} = 0, \quad -\tfrac{1}{2}\eta^2 f' + (\eta f s)' = 0, \tag{3.19}$$

where $u \equiv t^{-1/2}s(\eta)$. Conditions (3.8)–(3.9) become

$$s_+(\eta_G) = -\tfrac{1}{3}f^2 f', \quad f_+(\eta_G) = D, \quad s(\eta_N) = \tfrac{1}{2}\eta_N, \quad s'(\eta_N) = -\tfrac{1}{4}, \tag{3.20}$$

respectively. Finally, the equation of dynamic grounding-line control (3.10) becomes

$$D^2(f')^2 + \left(\eta_G + \frac{D^3}{3\eta_G}\right)f' - \frac{1}{4}D^2 - \int_{\eta_G}^{\eta_N} f\left(\frac{s}{\eta}\right)' \,\mathrm{d}\eta = 0. \tag{3.21}$$

We solve (3.15), (3.16a, b) and (3.19)–(3.21) using a fourth-order Runge-Kutta scheme in which both η_G and η_N are treated as shooting parameters. Our solution with $D = 2$, shown in figure 4(b), exhibits a convex frontal shape characteristic of the early-time extrusion due to a vertical line source (Pegler & Worster 2012). The similarity coordinate of the grounding line η_G, plotted as a function of D in figure 4(c), is seen to reduce sharply from the trend set by the solutions for $D < D_0$. For large D, η_G converges to zero, implying that the early-time flow of the shelf in this limit ultimately becomes equivalent to that produced by a vertical line source (Pegler & Worster 2012). By suitably rescaling our similarity variables to those used by Pegler & Worster (2012) and using the similarity coordinate for the frontal position that they determined, we find that

$$\eta_N \sim 1.71\, D^{-1/2} \qquad (D \to \infty). \tag{3.22}$$

This asymptotic relationship is plotted as a dotted curve in figure 4(c), where it is seen to agree closely with the numerical solution for $D \gtrsim 3$.

3.2. *Convergence towards steady flow*

The similarity solutions calculated above no longer apply once $t \sim 1$ and the dynamical influence of the horizontal forces exerted by the ocean become significant. To determine the subsequent evolution, we solve the full system (3.4)–(3.11) numerically using separate numerical schemes for the sheet and shelf. For the shelf, we integrate (3.6)–(3.9) along with (3.10) or (3.11) using the same Lagrangian scheme employed by Pegler & Worster (2012). For the sheet, we integrate (3.4)–(3.5) using an implicit finite-difference scheme of second order in which the time-dependent numerical domain $[0, r_G(t)]$ is mapped onto the fixed domain $[0, 1]$ with the transformation $R \equiv r/r_G(t)$. We initialize the integration using the early-time similarity solutions calculated in §3.1 above.

Our numerical solutions, illustrated earlier in figure 2, show that the flow of the sheet, grounding line and shelf converge towards a steady state near the source but the front of the shelf remains time-dependent with

$$r_G \sim \mathrm{func}(D), \qquad r_N \sim 0.433\, t \qquad (t \to \infty). \tag{3.23a,b}$$

The frontal propagation (3.23b) is equivalent to that describing the late-time self-similar propagation of a layer produced radially by a vertical line source (Pegler & Worster 2012). This equivalence is a consequence of the fact that, beyond a characteristic distance in front of the grounding line, the onset of buoyancy-induced flow causes the shelf to lose knowledge of the details associated with its inflow boundary condition (3.8a, b).

We compute the steady states directly by setting the time derivatives in (3.4), (3.7) and (3.10) to zero. Integrating the resulting form of (3.4) subject to (3.5a), we determine that

$$rq = -\tfrac{1}{3} rH^3 H' = 1 \tag{3.24}$$

uniformly throughout the sheet, where $H = H(r)$ only and we have used a prime here to denote $\mathrm{d}/\mathrm{d}r$. Integrating (3.24) further subject to (3.5b), we obtain

$$H = [D^4 + 12\ln(r_G/r)]^{1/4}, \tag{3.25}$$

where r_G is the, as-yet-undetermined, steady-state position of the grounding line. The asymptotic steady-state (3.25) is shown as a dotted curve in figures 2(a, b) for $r < r_G$, where it is seen to contain a point of inflexion if $D = 1$, but not if $D = 2$.

Integrating the steady form of (3.7) and applying (3.24) and (3.8a, b), we determine that

$$rq = rHu = 1 \tag{3.26}$$

uniformly throughout the shelf. Using (3.26) to eliminate u in (3.6), we obtain

$$-HH'' + H'^2 + \frac{HH'}{2r} = \frac{1}{4} rH^3 H', \tag{3.27}$$

(Pegler & Worster 2012). We consider solutions to (3.27) subject to

$$H(r_G) = D, \qquad \lim_{r\to\infty}(rH) = \sqrt{6}, \tag{3.28a,b}$$

which are (3.8a) and a condition that matches the flow to a far field in which the layer is both steady and subject to zero stress at its front (Pegler & Worster 2012).

To calculate the remaining unknown r_G, which acts as a parameter in the steady-state profiles of the sheet and shelf obtained above, we consider the steady form of (3.10), namely,

$$\left(2H^2H'^2 - \frac{2q}{r_G}\right) - \frac{1}{2}H^2 - 2\int_{r_G}^{\infty} H\frac{\mathrm{d}}{\mathrm{d}r}\left(\frac{u}{r}\right)\mathrm{d}r = 0 \qquad (r = r_G), \tag{3.29}$$

which is equivalent to the dimensionless form of the dynamic condition (2.21) with $\boldsymbol{\nabla}\cdot\boldsymbol{q} = 0$. Using (3.24) to evaluate q and H' in (3.29), and using (3.26) to eliminate u in the integrand of the buttressing integral, we obtain

$$A + F_0 + B \equiv \frac{2}{r_G^2}\left(\frac{9}{D^4} - 1\right) - \frac{1}{2}D^2 - 2\int_{r_G}^{\infty} H\frac{\mathrm{d}}{\mathrm{d}r}\left(\frac{1}{r^2H}\right)\mathrm{d}r = 0, \tag{3.30}$$

where we have labelled the respective terms the *rate of advection* A, the *buoyancy force* F_0 and the *buttressing* B.

The steady-state buttressing $B = B(D, r_G)$ in (3.30) depends on the solution to the shelf equations (3.27)–(3.28) and is therefore a function of the two variables D and r_G, appearing in the inlet condition (3.28a). However, this dependence can be reduced to a single parameter formed from a particular combination of D and r_G by first recasting (3.27)–(3.28a, b) and (3.30) in terms of the scaled variables

$$\tilde{r} \equiv Dr, \qquad \tilde{H} \equiv H/D. \tag{3.31}$$

In terms of (3.31), the steady-state shelf equation (3.27) and conditions (3.28a, b) become

$$-\tilde{H}''\tilde{H} + \tilde{H}'^2 + \frac{\tilde{H}\tilde{H}'}{2\tilde{r}} = \frac{1}{4}\tilde{r}\tilde{H}^3\tilde{H}', \qquad \tilde{H}(\tilde{r}_G) = 1, \quad \lim_{\tilde{r}\to\infty}(\tilde{r}\tilde{H}) = \sqrt{6}, \tag{3.32}$$

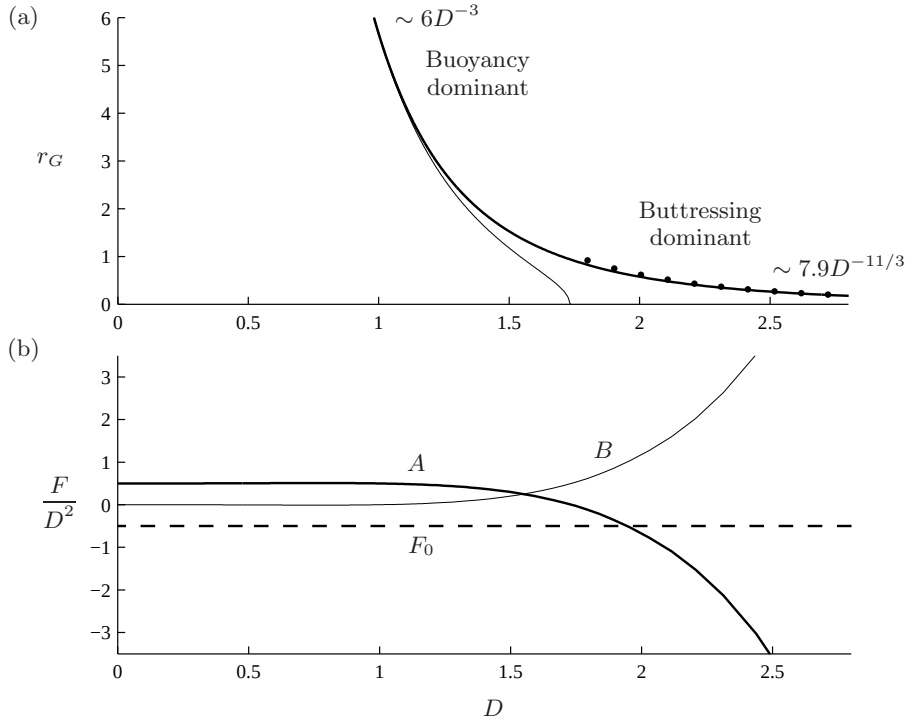

FIGURE 5. (a) Steady position of the grounding line r_G plotted against the dimensionless flotation thickness D. The position (3.36) that would result without buttressing ($B = 0$) is plotted as a thin curve. The asymptote (3.35) for $D \gg 1$ is plotted as a dotted curve. (b) The steady-state rate of advection A (thick), the buoyancy force F_0 (dashed) and the buttressing B (thin), defined in (3.30), that act at the grounding line, each scaled by D^2.

respectively, and (3.30) becomes

$$4(9D^{-4} - 1) = \tilde{r}_G^2\big[1 - 2\tilde{B}(\tilde{r}_G)\big], \tag{3.33}$$

$$\text{where} \quad \tilde{B}(\tilde{r}_G) \equiv -2\int_{\tilde{r}_G}^{\infty} \tilde{H}\frac{\mathrm{d}}{\mathrm{d}\tilde{r}}\left(\frac{1}{\tilde{r}^2\tilde{H}}\right)\mathrm{d}\tilde{r} \tag{3.34}$$

is the scaled buttressing exerted by a steady-state shelf produced at a grounding line of scaled radius $\tilde{r}_G$ (Pegler & Worster 2012). The rescaled system (3.32)–(3.34) now depends only on the single parameter $\tilde{r}_G \equiv Dr_G$. Having obtained the function $\tilde{B}(\tilde{r}_G)$ by numerically integrating (3.32) using a fourth-order Runge-Kutta scheme, we solve the remaining algebraic equation (3.33) for $\tilde{r}_G(D)$ using a numerical root finder. In terms of our original dimensionless variables, the grounding-line position is then given by $r_G \equiv \tilde{r}_G/D$.

As shown in figure 5(a), our computed steady-state grounding-line positions r_G are inversely related to the dimensionless flotation thickness D. The steady-state forces at the grounding line, defined in (3.30), are each plotted in figure 5(b) in forms scaled by D^2. For small values of $D \lesssim 1$, the buoyancy force F_0 provides the dominant contribution to the force exerted onto the sheet ($F_0 \gg B$). At larger values, however, buttressing becomes significant for $D \gtrsim 1.5$ and dominant ($F_0 \ll B$) for $D \gtrsim 2.5$. These limiting balances reflect the fact that buttressing B decays to zero in the limit of large grounding-line curvature ($\tilde{r}_G \to \infty$), but tends to infinity in the opposite limit ($\tilde{r}_G \to 0$), while the

buoyancy force $F_0 \equiv (1/2)D^2$, being independent of r_G, remains the same in either limit (Pegler & Worster 2012). We determine an asymptotic approximation for the grounding-line position in cases where the force balance is dominated by buttressing ($D \to \infty$) by substituting the small-$\tilde{r}_G$ approximation for $\tilde{B}$ obtained by Pegler & Worster (2012) into (3.34) to yield

$$r_G \sim 7.9 D^{-11/3} \qquad (D \to \infty), \tag{3.35}$$

which we have plotted as a dotted curve in figure 5(a), where it is seen to agree closely with the numerical solution if $D \gtrsim 2$.

We assess the importance of buttressing B on the grounding-line position by comparing the steady-state value of r_G obtained above with the corresponding value obtained if buttressing is set to zero ($B = 0$). The resulting state is applicable to the geophysical situation where the ice shelf calves immediately at the grounding line. With $B = 0$, the steady-state grounding-line position can be determined analytically from (3.30) as

$$r_{G0} = 2D^{-1}(9D^{-4} - 1)^{1/2} \qquad (B = 0), \tag{3.36}$$

which we have plotted as a thin, solid curve in figure 5. Comparing (3.36) with the position r_G determined above, we see that the general influence of buttressing B is to cause the grounding line to approach a more advanced position. Notably, the position without buttressing (3.36) vanishes at $D = \sqrt{3}$, implying that, for $D > \sqrt{3}$, an overextended grounding line with no buttressing would retreat back towards the source before detaching completely from the bedrock. For such values of D, buttressing prevents the ultimate detachment of the sheet from the bedrock.

A particular property of the buttressing B developed by a radially flowing ice shelf is that it approaches a finite, steady-state value, despite the extent of the shelf continuing to grow indefinitely (Pegler & Worster 2012). In other geometries, such as that of a channel (Pegler *et al.* 2013), the buttressing can increase without limit, causing the flow to instead remain time-dependent, with a grounding line that advances indefinitely.

It is notable that, while our results show that a radially spreading marine ice sheet converges towards a steady state on horizontal bedrock, the analogous two-dimensional geometry (cf. Weertman 1974) does not allow this. The fundamental difference is not a consequence of buttressing, as evidenced by the existence of the unbuttressed steady-state solutions (3.36), but is instead related to the fact that the steady-state rate of advection A in (3.30) depends on r_G, allowing (3.30) to be satisfied for a distinguished value of r_G. This is not true in two-dimensions, where the uniformity of the steady-state, depth-integrated velocity q can be shown to cause A to take a value that is independent of the grounding-line position. All the terms in the two-dimensional analogue of (3.30) are therefore independent of the grounding-line position, implying that it cannot generally be satisfied. We can speculate that a stable, steady-state grounding-line position can occur more generally on bedrock that slopes upwards in the radial direction, as is characteristic in West Antarctica (Bamber *et al.* 2009).

Given typical kinematic viscosities $\nu \approx 10^{10} - 10^{13}\,\mathrm{m^2\,s^{-1}}$, fluxes $Q_0 \approx 10 - 100\,\mathrm{m^3\,s^{-1}}$, and flotation thicknesses $d_0 \approx 500 - 2000\,\mathrm{m}$ characteristic of ice sheets (Paterson 1994), we evaluate an order-of-magnitude estimate of the dimensionless flotation thickness (3.13) to be in the range

$$D \equiv d_0 \left(\frac{2\pi g}{\nu Q_0}\right)^{1/4} \approx 0.3 - 10. \tag{3.37}$$

This spans cases for which our theoretical model predicts that the position of the grounding line is controlled by hydrostatic forces and those for which it is controlled by the but-

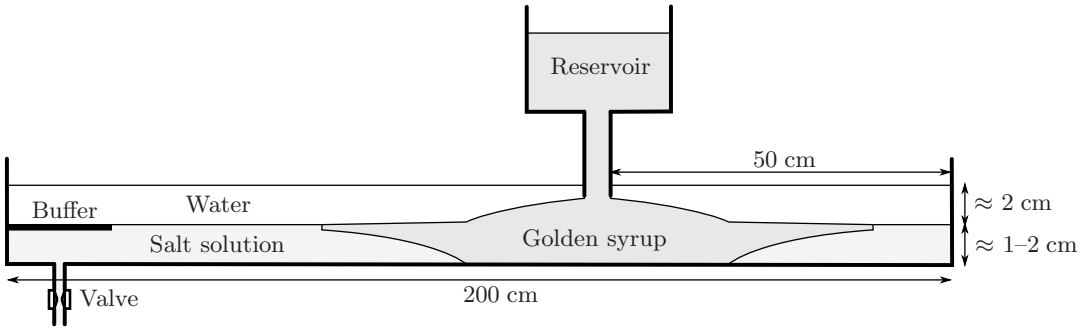

FIGURE 6. Schematic of our experimental system.

tressing exerted by the shelf. The buttressing developed by radial flow therefore has the potential to play an important role in controlling the dynamics of grounding lines. Note that, in calculating the estimate (3.37), any variations either in the effective kinematic viscosity of ice ν, owing to its non-Newtonian rheology (Paterson 1994), or in the entry flux Q_0, are relatively unimportant because both are raised to quarter powers. By far the most influential parameter is the flotation thickness d_0.

4. Experimental study

We have conducted a series of laboratory experiments with which to compare aspects of our theoretical predictions. Our experiments were conducted in a Perspex tank 200 cm long, 110 cm wide and 5 cm deep, shown schematically in figure 6. We used golden syrup to form the viscous current and denser solutions of potassium carbonate to form the inviscid fluid (cf. Robison *et al.* 2010; Pegler & Worster 2012; Pegler *et al.* 2013). To effectively eliminate the influence of surface tension acting at the front of the current, we arranged a layer of water above the solution, such that the viscous fluid would flow along the interface between the water and the solution (cf. Pegler & Worster 2012). As in that study, the presence of the inviscid upper layer can be accommodated straightforwardly into the theoretical model by using the generalized formula for the reduced gravity

$$g' \equiv \frac{(\rho_w - \rho)(\rho - \rho_a)}{(\rho_w - \rho_a)\rho} g, \tag{4.1}$$

where $\rho_a \approx 1.00\,\mathrm{g\,cm^{-3}}$ is the density of water. The introduction of the upper layer of water could be observed to smear the density profile slightly between the water and the solution over a depth of the order of a millimetre (cf. Pegler & Worster 2012).

The kinematic viscosity ν of the syrup was measured before each experiment using a falling-sphere method, to an estimated accuracy of $5\,\mathrm{cm^2\,s^{-1}}$, and varied slightly between our experiments owing to changes in temperature. The density of the syrup ($\rho \approx 1.439\,\mathrm{g\,cm^{-3}}$) and the solution ($\rho_w \approx 1.462$ to $1.551\,\mathrm{g\,cm^{-3}}$) were each measured using a hydrometer to an accuracy of $0.001\,\mathrm{g\,cm^{-3}}$, giving the reduced gravity (4.1) to an accuracy of $1\,\mathrm{cm\,s^{-2}}$. We used a method of injection of syrup identical to that of Pegler & Worster (2012), whereby a reservoir and tube, initially in contact with the base of the tank, were raised to initiate the injection. Before each experiment, the volumetric flux Q_0 of the delivery system was measured to an estimated accuracy of $0.1\,\mathrm{cm^3\,s^{-1}}$ by measuring the time taken for it to supply a known volume of syrup. To counteract the rise in the level of the solution caused by its displacement by the intruding syrup, we extracted solution manually through a valve-controlled exit pipe at a rate which approximated that

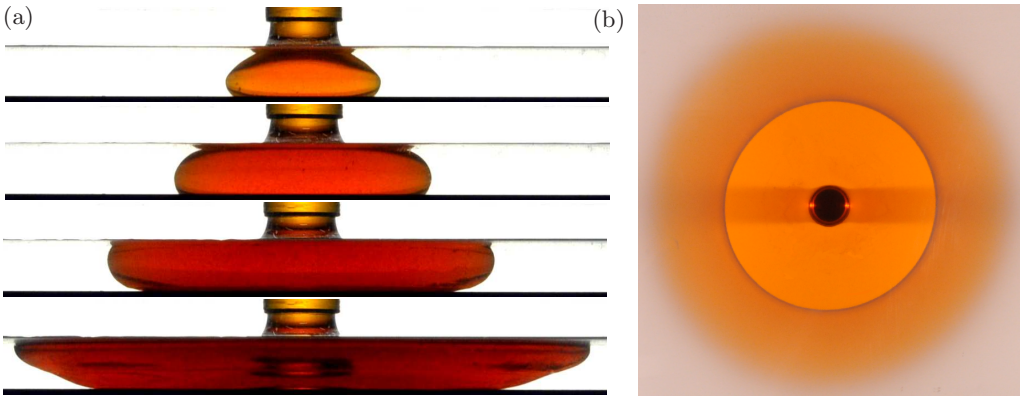

FIGURE 7. (a) Sequence of photographs of an experiment viewed from the side at times $t = 5, 20, 50$ and $100\,\mathrm{s}$ after the initiation of the injection; and (b) a photograph of an experiment viewed from below the tank, showing the sharp contrast between the grounded and floating parts of the flow. An upper layer of water was not included in the experiment used to take the photographs in (a) because of the optical distortion it would have caused. The experiment shown in (a) also features in supplementary movie 1.

at which the syrup was injected (cf. Pegler *et al.* 2013). Errors in the extraction process were mitigated by using a tank with a relatively large surface area, providing a constant depth to within an estimated tolerance of 0.03 cm over the course of each experiment. Any unintended extraction of the water layer above the outlet was prevented by securing a buffer between the outlet and the interface.

The experiment was recorded using a camera directed to view the underside of the tank via an angled mirror beneath it. To create a visual contrast between the grounded sheet and the floating shelf, we increased the opacity of the salt solution by adding a white pigment of titanium dioxide to it. This partially obscured the shelf, creating a strong contrast between the grounded sheet and the floating shelf, as shown in figure 7(b). A sequence of photographs of one experiment viewed from the side is shown in figure 7(a) and supplementary movie 1.

As shown in table 1, our experimental parameters spanned viscosities ν from 490 to $550\,\mathrm{cm^2\,s^{-1}}$, reduced gravities g' from 15 to $61\,\mathrm{cm\,s^{-2}}$, input fluxes Q_0 from 7.2 to $9.2\,\mathrm{cm^3\,s^{-1}}$ and depths of the inviscid fluid b_0 from 0.90 to 1.67 cm. In figure 8, we have plotted the experimental position of the grounding line $r_G(t)$ (crosses) and of the shelf front $r_N(t)$ (dots) as functions of time, with each compared to the corresponding theoretical predictions (solid curves). Some agreement is observed between the predictions and the data at early times ($t \lesssim 100\,\mathrm{s}$) in each experiment. However, while the theory predicts that the grounding line in each experiment should have converged to a steady position by $t \approx 300\,\mathrm{s}$ in each experiment, the experimental grounding-line positions did not do this, instead continuing to advance with a rate of expansion that was still significant at the end of each experiment ($t > 500\,\mathrm{s}$). Although some gradual reduction in grounding-line velocity with time is evident, there is little indication that the experimental grounding lines were converging towards steady states.

The experimental positions of the shelf front r_N nevertheless agree well with the theoretical predictions at early times, with their gradual reduction below the theoretical curve at later times likely to be a consequence of the slight smearing of the density profile at the interface between the water and the solution (Pegler & Worster 2012).

Experiment	ν ($\mathrm{cm}^2\,\mathrm{s}^{-1}$)	g' ($\mathrm{cm}\,\mathrm{s}^{-2}$)	Q_0 ($\mathrm{cm}^3\,\mathrm{s}^{-1}$)	b_0 (cm)	D
(a)	515	57	9.2	0.90	0.88
(b)	490	61	9.2	1.14	1.14
(c)	500	28	7.6	1.40	1.29
(d)	550	15	7.2	1.67	1.44

TABLE 1. Parameter values used in our experiments.

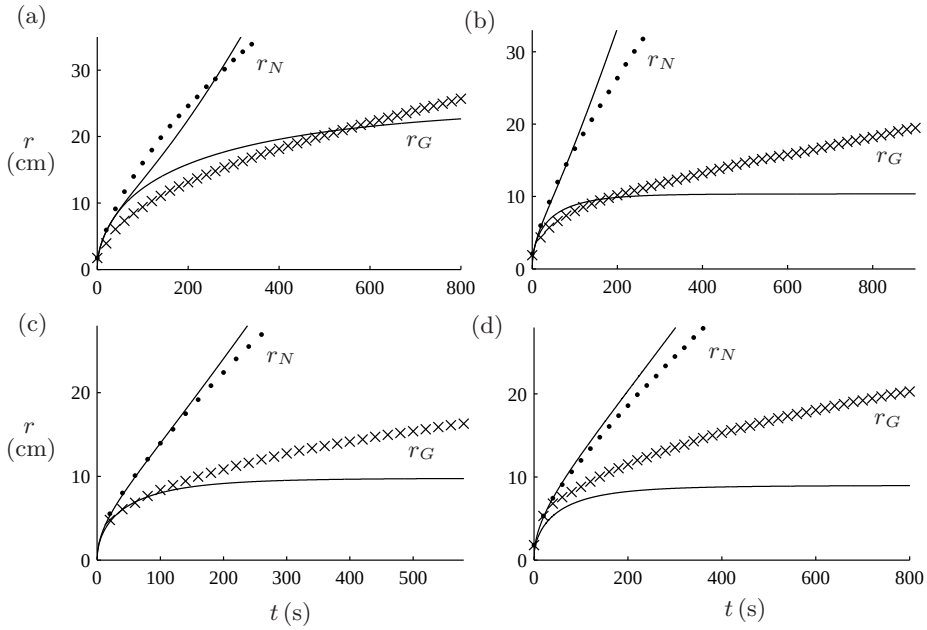

FIGURE 8. The experimental data for the position of the grounding line r_G (crosses) and the shelf front r_N (dots) as functions of time, compared with the theoretical predictions (solid curves). Each panel represents a separate experiment whose parameters are given in table 1.

5. Discussion

The significant discrepancy between the relatively rapid convergence towards steady flow predicted by our theory and the continued advancement of the grounding lines in our experiments is suggestive of a fundamental mismatch between the model and the experimental flow. With no obvious errors or extraneous physics of any significance in our experiments, we expect the discrepancy to be a consequence of one or more of the approximations used to develop our theoretical model.

Our modelling assumptions comprise a general thin-film approximation and two distinct approximations that relate specifically to our treatment of the flow across the grounding line. The former underlies both the shear-dominated regime of the sheet presented in §2.1 and the extensional flow regime of the shelf in §2.2. These regimes have each been independently compared successfully with experimental data over aspect ratios characteristic of our experiments (Huppert 1982; Pegler & Worster 2012). Therefore, we do not expect our use of a thin-film approximation in regions away from the grounding line to introduce any significant discrepancy. Instead, we expect the discrepancy to relate to our treatment of the flow across the grounding line.

In modelling the flow across the grounding line, we make two main approximations.

One relates to our uniform neglect of extensional stresses in the sheet, leading to an effective patching of the forces between the upstream, shear-dominated region of the sheet and the extensional shelf (2.17). It has been shown, by comparing the predictions of a similar model that neglects extensional stresses up to the grounding line and another that includes them, that there are no significant quantitative differences between the two, with only a very slight, though formally order-unity, adjustment to the predicted value of $\boldsymbol{\nabla \cdot q}$ (Pegler 2012). Hence, this particular approximation appears unlikely to account for the kind of significant and persistently increasing discrepancies seen between the predictions and the data.

The second approximation we make relates to the uniform neglect of viscous bending stresses throughout the system. Such stresses, represented in two dimensions by the $\partial\sigma_{xz}/\partial x$ term in the vertical component of the Stokes equations, can be shown to be negligible both in the shear-dominated regime of the sheet, where only vertical-shear stresses are important (Huppert 1982), and in the extensional regime of the shelf, where it is the only component of the stress tensor that can be formally neglected (DiPietro & Cox 1979; MacAyeal 1989; Howell 1996; Pegler & Worster 2012). In both regimes, the absence of significant bending stresses depends on the lack of any dramatic change in the vertical-shear profile of the flow in the horizontal direction. However, such a dramatic change would seem likely to occur at the grounding line, with the sudden transition from no-slip to free-slip at the base of the current leading to significant horizontal gradients in vertical shear. Such gradients act to bend the flow downwards in the manner of a viscous beam (Ribe 2001; Schoof 2011) or the swelling of a viscous flow out of a pipe (Richardson 1970). It is plausible that such bending drives a significant portion of the flow downwards to intersect the base of the tank in front of the grounding line, causing its advance to persist for longer than predicted by our model. A more extensive study is needed to investigate the role of such dynamics.

6. Conclusions

We have developed a theoretical model for a radially flowing marine ice sheet and compared its predictions with data from an analogue laboratory study. The theoretical predictions and the experimental observations showed some agreement at early times, but significant discrepancy in the transitional behaviour at late times indicates that certain physics not included in our theoretical model could have significant implications for the dynamics of grounding lines. In particular, the discrepancy may highlight the significance of viscous bending stresses, which are not accounted for in the shallow ice models that are commonly used to model ice sheets.

Despite the discrepancies found between our predictions and experiments, our model illustrates several new phenomena associated with the flow of grounding lines in three dimensions. One such aspect relates to the potential for the buttressing due to the ice shelf, which here originates from viscous hoop stresses, to dominate the dynamics of the grounding line. The relative significance of buttressing compared with hydrostatic forces was shown to be characterized by a dimensionless flotation thickness $D \equiv d_0(\nu g/2\pi Q_0)^{1/4}$. For sufficiently large values of D, our model predicts that the buttressing due to hoop stresses can intervene to prevent a complete detachment of the ice sheet from the bedrock.

Previous two-dimensional studies have shown that grounding lines are unstable on horizontal bedrock (Weertman 1974). Our results suggest that this is not generally true in three dimensions, where the influence of radial spreading causes the steady-state flux per unit width of the flow delivered by the sheet to decay with the grounding-line position, leading instead to its convergence towards a steady position.

We are grateful to the technicians of the DAMTP laboratory for assistance in setting up our experiments. S.S.P. acknowledges the support of an EPSRC doctoral studentship.

REFERENCES

Alley, R. B. & Bindschadler, R. A. 2001 The West Antarctic Ice Sheet: Behavior and Environment. *Antarct. Res. Ser.* **77**.

Bamber, J. L., Riva, R. E. M., Vermeersen, B. L. A. & LeBrocq, A. M. 2009 Reassessment of the potential sea-level rise from a collapse of the West Antarctic Ice Sheet. *Science* **324** (5929), 901–903.

DiPietro, N. D. & Cox, R. G. 1979 The spreading of a very viscous liquid on a quiessent water surface. *Quart. J. Mech. Appl. Math.* **32**, 355–381.

Fowler, A. C. & Larson, D. A. 1978 On the flow of polythermal glaciers. I. Model and preliminary analysis. *Proc. R. Soc.* **363**, 217–242.

Howell, P. D. 1996 Models for thin viscous sheets. *Eur. J. Appl. Math* **7**, 321–343.

Huppert, H. E. 1982 The propagation of two-dimensional and axisymmetric viscous gravity currents over a rigid horizontal surface. *J. Fluid Mech.* **121**, 43–58.

MacAyeal, D. R. 1989 Large-scale ice flow over a viscous basal sediment: Theory and application to Ice Stream B, Antarctica. *J. Geophys. Res.* **94**, 4071–4087.

Nowicki, S. M. J. & Wingham, D. J. 2008 Conditions for a steady ice sheet–ice shelf junction. *Earth Planet Sci. Lett.* **265**, 246–255.

Paterson, W. S. B. 1994 *The physics of glaciers*, 3rd edn. Pergamon.

Pegler, S. S. 2012 The fluid mechanics of ice-shelf buttressing. PhD thesis, University of Cambridge.

Pegler, S. S., Kowal, K. N., Hasenclever, L. Q. & Worster, M. G. 2013 Lateral controls on grounding-line dynamics. *J. Fluid Mech.* **722**, R1.

Pegler, S. S., Lister, J. R. & Worster, M. G. 2012 Release of a viscous power-law fluid over a denser inviscid ocean. *J. Fluid Mech.* **700**, 63–76.

Pegler, S. S. & Worster, M. G. 2012 Dynamics of a viscous layer flowing radially over an inviscid ocean. *J. Fluid Mech.* **696**, 152–174.

Ribe, N. M. 2001 Bending and stretching of thin viscous sheets. *J. Fluid Mech.* **433**, 135–160.

Richardson, S. 1970 A 'stick-slip' problem related to the motion of a free jet at low Reynolds numbers. *Proc. Cambridge Philos. Soc.* **67**, 477–489.

Robison, R. A. V., Huppert, H. E. & Worster, M. G. 2010 Dynamics of viscous grounding lines. *J. Fluid Mech.* **648**, 363–380.

Schoof, C. 2007 Marine ice sheet dynamics. Part 1: The case of rapid sliding. *J. Fluid Mech.* **573**, 27–55.

Schoof, C. 2011 Marine ice sheet dynamics. Part 2: A Stokes flow contact line problem. *J. Fluid Mech.* **679**, 122–255.

Weertman, J. 1957 Deformation of floating ice shelves. *J. Glac.* **3**, 38–42.

Weertman, J. 1974 Stability of the junction of an ice sheet and an ice shelf. *J. Glac.* **31**, 3–11.

Wilchinsky, A. V. & Chugunov, V. A. 2000 Ice stream–ice shelf transition: theoretical analysis of two-dimensional flow. *Ann. Glaciol.* **30**, 153–162.

Wingham, D., Wallis, D. & Shepherd, A. 2009 Spatial and temporal evolution of Pine Island Glacier thinning. *Geophys. Res. Lett.* **36**, L17 501.